Liquid Crystals
Publication details, including instructions for authors and subscription information:
http://www.informaworld.com/smpp/title~content=t713926090

Phase behaviour of the thermotropic cubic mesogen 1,2-bis(4-*n*-decyloxybenzoyl)hydrazine under pressure

Yoji Maeda Corresponding author[a]; Takeya Ito[b]; Shoichi Kutsumizu[b]
[a] Nanotechnology Research Institute, National Institute of Advanced Industrial Science and Technology, Ibaraki 305-8565, Japan [b] Department of Chemistry, Faculty of Engineering, Gifu University, Gifu 501-1193, Japan

Online publication date: 25 May 2010

To cite this Article Maeda Corresponding author, Yoji , Ito, Takeya and Kutsumizu, Shoichi(2004) 'Phase behaviour of the thermotropic cubic mesogen 1,2-bis(4-*n*-decyloxybenzoyl)hydrazine under pressure', Liquid Crystals, 31: 5, 623 — 632
To link to this Article: DOI: 10.1080/02678290410001675156
URL: http://dx.doi.org/10.1080/02678290410001675156

LIQUID CRYSTALS, VOL. 31, NO. 5, MAY 2004, 623–632

Taylor & Francis
Taylor & Francis Group

Phase behaviour of the thermotropic cubic mesogen 1,2-bis(4-*n*-decyloxybenzoyl)hydrazine under pressure

YOJI MAEDA*

Nanotechnology Research Institute, National Institute of Advanced Industrial Science and Technology, Higashi 1-1, Tsukuba, Ibaraki 305-8565, Japan

TAKEYA ITO and SHOICHI KUTSUMIZU

Department of Chemistry, Faculty of Engineering, Gifu University, 1-1 Yanagido, Gifu 501-1193, Japan

(*Received 14 November 2003; accepted 18 January 2004*)

The phase transition behaviour of an optically isotropic, thermotropic cubic mesogen 1,2-bis(4-*n*-decyloxybenzoyl)hydrazine, BABH(10), was investigated under pressures up to 300 MPa using a high pressure differential thermal analyser, a wide angle X-ray diffractometer and a polarizing optical microscope (POM) equipped with a high pressure optical cell. The reversible change in structure and optical texture between the cubic (Cub) and smectic C (SmC) phases was associated with a change from a spot-like X-ray pattern and dark field for the Cub phase to the Debye–Sherrer ring pattern and sand-like texture for the SmC phase under both isobaric and isothermal conditions. The Cub phase was found to disappear at pressures above about 11 MPa. The phase transition sequence, low temperature crystal (Cr_3)–intermediate temperature crystal (Cr_2)–high temperature crystal (Cr_1)–Cub–SmC–isotropic liquid (I) observed at atmospheric pressure, is maintained in the low pressure region below 10 MPa. The transition sequence changes to Cr_3–Cr_2–(Cr_1)–SmC–I in the high pressure region. Since the Cub–SmC transition line determined by POM has a negative slope (dT/dP) in the T–P phase diagram, a triple point is estimated approximately at 10–11 MPa, and 143–145°C for the SmC, Cub and Cr_1 phases, giving the upper limit of pressure for the observation of the cubic phase.

1. Introduction

Research into thermotropic cubic liquid crystalline phases started in 1957, when Gray *et al.* reported the synthesis of 4′-*n*-hexadecyloxy- and 4′-*n*-octadecyloxy-3′-nitrobiphenyl-4-carboxylic acids [1]. In 1978, 1,2-bis(4-*n*-alkyloxybenzoyl)hydrazines, referred to as BABH(*n*) with *n* indicating the number of carbon atoms in the alkoxy chain, were synthesized by Schubert *et al.* [2]. The octyloxy-, nonyloxy- and decyloxy-homologues exhibit both cubic (Cub) and smectic C (SmC) phases; their phase sequence is (Cr_I–Cr_{II} or Cr_I–Cr_{II}–Cr_{III})–Cub–SmC–isotropic liquid (I) [3]. The chemical structure of 1,2-bis(4-*n*-decyloxybenzoyl)hydrazine BABH(10) is:

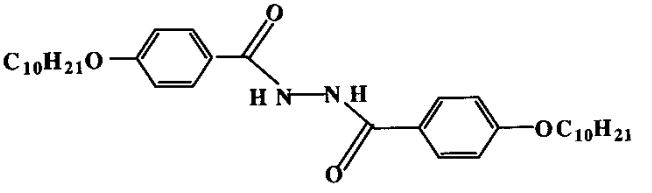

Göring *et al.* [4] determined the crystal structure of BABH(8) as well as the structures of the Cub and SmC phases. The molecules in the crystalline phase form sheets linked by hydrogen bonds between the neighbouring molecules, and the Cub phase has a body centered cubic cell (its cell parameter $a = 6.46$ nm) with a space group *Ia*3*d*. The jointed-rod model for the *Ia*3*d* space group, i.e. two interwoven but unconnected networks of rods linked three by three [5–8], was suggested for the Cub phase of BABH(8). Precise

*Author for correspondence; e-mail: yoji.maeda@aist.go.jp

Liquid Crystals ISSN 0267-8292 print/ISSN 1366-5855 online © 2004 Taylor & Francis Ltd
http://www.tandf.co.uk/journals
DOI: 10.1080/02678290410001675156

calorimetric measurements of BABH(8) were carried out by Sorai and his collaborators [9], and provide reliable thermodynamic quantities of the phase transitions. Saito *et al.* [10, 11] discussed the phase diagrams of several cubic liquid crystalline compounds in terms of the number of carbon atoms in the alkyl chains.

One of the present authors (Y.M.) reported the interesting phase behaviour of BABH(8) under hydrostatic pressure using a high pressure differential thermal analyser (DTA) and a polarizing optical microscope (POM) equipped with a high pressure optical cell, and determined the T vs. P phase diagram in the heating mode [12]. The Cub phase was found to disappear at pressures above about 30 MPa. The phase transition sequence, low temperature crystal (Cr_2)–high temperature crystal (Cr_1)–Cub–SmC–I observed in the low pressure region changes to Cr_2–SmC–I in the high pressure region. Since only the Cub–SmC transition line of the phase boundaries has a negative slope (dT/dP) in the T–P phase diagram, the temperature range for the Cub phase decreases rapidly with pressure. As a result, a triple point was estimated approximately as 31.6 MPa, 147°C for the SmC, Cub and Cr_1 phases, indicating the upper limit of pressure for Cub phase formation. The reversible changes in structure and optical texture between the Cub and SmC phases were associated with changes from a spot-like X-ray pattern and dark field for the Cub phase to the Debye–Sherrer ring pattern and sand-like texture for the SmC phase both in isobaric and isothermal experiments. BABH(10) also shows Cub and SmC phases similar to BABH(8) [3]. The interesting phase behaviour of BABH(8) under pressure prompted us to extend the study to the phase behaviour of BABH(10) under hydrostatic pressure, particularly focused on the effect of pressure on the phase stability of the Cub phase.

In this paper, we present experimental results on the thermal, morphological and structural behaviour of BABH(10) under hydrostatic pressures up to 300 MPa using a high pressure DTA, a POM equipped with a high pressure optical cell, and a wide angle X-ray diffractometer (WAXD) equipped with a high pressure vessel.

2. Experimental

2.1. *Sample characterization under ambient pressure*

BABH(10), prepared as described in [2], was used in this study. Samples had been recrystallized from ethanol several times and the purity was confirmed by infrared (IR), ^{1}H NMR and mass spectroscopies, and elemental analysis. Thermal characterization of BABH(10) was performed on Perkin-Elmer DSC-7 and Seiko Instruments SSC-5000 differential scanning calorimeters at a scanning rate of 5°C min^{-1} under N_2 gas flow. Temperatures and heats of transition were calibrated using standard materials (indium and tin). Transition temperatures were determined as the onset of the transition peaks at which the tangential line of the inflection point of the rising part of the peak crosses the extrapolated baseline. Morphological characterization was performed using a Leiz Orthoplan polarizing optical microscope (POM) equipped with a Mettler hot stage FP-82.

2.2. *DTA measurements under pressure*

The high pressure DTA apparatus used in this study is described elsewhere [13]. The DTA system was operated in a temperature region between room temperature and 250°C under hydrostatic pressures up to 300 MPa. Dimethylsilicone oil with a medium viscosity (100 cSt) was used as the pressurizing medium. The sample weighing about 4 mg was put in the sample cell and coated with epoxy adhesive, to fix the sample in the bottom of the cell and also to prevent direct contact with the silicone oil. A fresh specimen of BABH(10) was used for each DTA measurement. The DTA runs were performed at a constant heating rate of 5°C min^{-1} under various pressures. Peak temperatures were taken as transition temperatures for constructing the real temperature vs. pressure phase diagram. When estimating specific points such as a triple point, the transition temperature was corrected to become the onset temperature by subtracting a temperature difference between the onset and peak temperatures, approximately 3.5°C.

2.3. *Morphological and X-ray characterization under pressure*

The optical texture observation of BABH(10) under hydrostatic pressure was performed using a Leitz Orthoplan POM equipped with a high pressure optical cell system [14]. Transmitted light intensity through the POM with crossed Nicols was recorded using a Mettler FP-90 photomonitor under atmospheric and hydrostatic pressures. The texture observation was performed under isobaric and isothermal conditions in the pressure range up to 50 MPa.

The structural change during the phase transition of BABH(10) under pressure was examined using a high pressure wide angle X-ray diffraction (WAXD) apparatus [13]. The high pressure vessel was set on the wide angle goniometer of a 12 kW rotating anode X-ray generator (Rotaflex RU200, Rigaku Co.). The sample was inserted into the vertical hole of the beryllium spindle as the sample cell. The beryllium spindle was mechanically compressed for pressure sealing using upper and lower pressure blocks. Then the sample was

pressurized hydrostatically at pressures up to 200 MPa. Ni-filtered Cu K_α X-ray irradiation was used and the diffraction patterns were recorded using an imaging plate detector (BAS-IP $127 \times 127\,mm^2$, Fuji Photo Film Co.).

3. Results and discussion

3.1. *Thermal and morphological observations under atmospheric pressure*

Figure 1 shows the DSC heating and cooling curves of BABH(10), in which one can see four sharp endothermic peaks in the heating curve and corresponding exothermic, slightly broader, peaks in the cooling curve. Although the Cub–SmC transition peak was barely detected on the high sensitivity SSC 5000 calorimeter used, because of the small heat of transition, the exothermic peak of the SmC–Cub transition was more clearly detected in the cooling curve. Since the existence of the Cub–SmC transition was clearly confirmed by the POM observations (see later), the observed peaks are assigned to the low temperature crystal (Cr_3)–intermediate temperature crystal (Cr_2), Cr_2–high temperature cyrstal (Cr_1), Cr_1–Cub and the SmC–I transitions in order of increasing temperature, and the phase sequence is reversible with temperature. The thermodynamic quantities associated with the phase transitions are summarized in the table. The cubic phase of BABH(10) extends over a temperature range of about 12°C, about half that (c.18–24°C) for BABH(8) [3, 4, 12].

Figure 2 shows the POM micrographs of textures of BABH(10) on heating under atmospheric pressure. The crystalline texture (*a,b*) is maintained to high temperatures of about 138°C. The crystalline texture then changes to a black field of view for the cubic phase at about 140°C. The black field of view (*c*) for the cubic phase is transformed into a sea-island texture at 161°C (*d*), showing bright islands with sand-like texture in the dark sea of the cubic phase. The sand-like texture belongs to the SmC phase and grows with increasing temperature. The sand-like texture of the SmC phase (*e*) is predominant in the high temperature region between 161 and 165°C and finally disappears completely on the isotropization (*f*). It is noteworthy

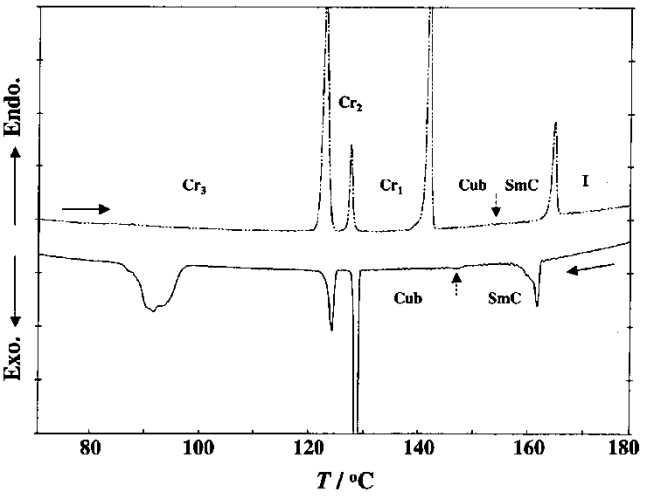

Figure 1. DSC heating and cooling curves of BABH(10). Scanning rate: 5°C min^{-1}.

that the texture of BABH(10) changes dramatically during the Cub–SmC transition, although this transition was barely detected by the DSC measurements. The morphological changes in texture are observed reversibly during the I–SmC–Cub–Cr transition sequence under atmospheric pressure. The POM transmitted light intensity vs. temperature curves of BABH(10) also clearly exhibited the transitions during heating and cooling.

3.2. *Morphological and structural observations under pressure*

Figure 3 shows the POM textures of BABH(10) on heating at 5 MPa. The crystalline texture is observed at temperatures up to about 140°C (*a* and *b*). When the crystal melts, the co-existing sea-island texture of bright islands and a dark sea appears at 145°C, corresponding to the SmC and cubic phases, respectively (*c*). The bright islands grow continuously and their area increases with temperature, indicating the gradual transition from the cubic phase to the SmC phase (*d*). The predominant sand-like texture (*e*) of the SmC phase disappears into the dark field of view for the isotropic liquid at 166°C (*f*). The morphological

Table. Thermodynamic quantities associated with the phase transitions of BABH(10).

Phase transition	T/°C	ΔH/kJ mol^{-1}	ΔS/J K^{-1} mol^{-1}	$(dT/dP)_{1atm}$	ΔV^a/cm^3 mol^{-1}
$Cr_3 \rightarrow Cr_2$	122.0	24.3	61.5	0.371_9	22.9
$Cr_2 \rightarrow Cr_1$	127.1	4.9	12.2	0.357_4	4.4
$Cr_1 \rightarrow$ Cub	141.2	23.1	55.7	0.285_5	15.9
Cub→SmC	153.0	0.4	0.9	-1.334_5	−1.2
SmC→I	163.9	7.2	16.4	0.305_0	5.0

[a] ΔV was deduced using the Clausius–Clapeyron equation (see text).

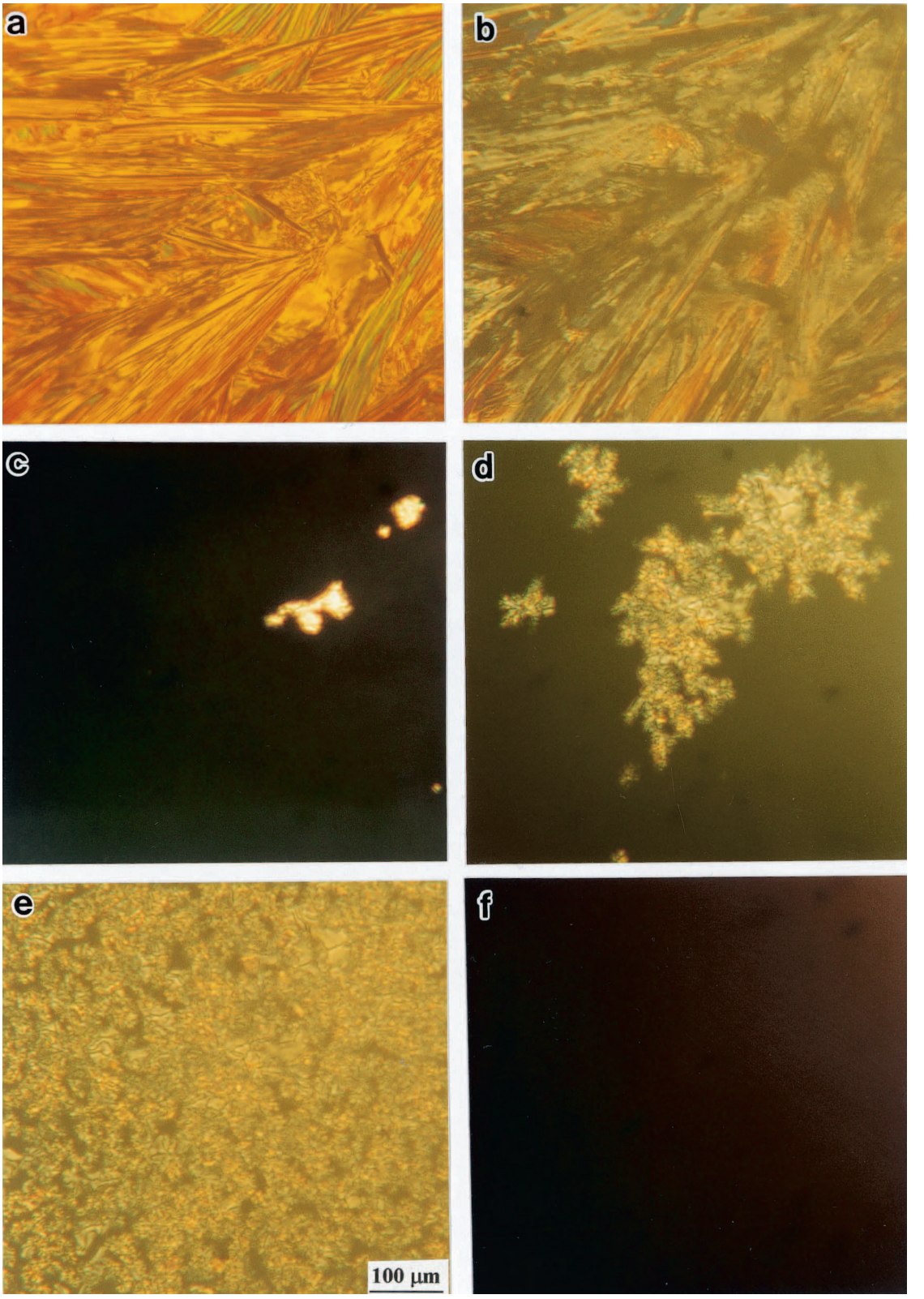

Figure 2. POM micrographs of BABH(10) on heating at atmospheric pressure: (*a*) Cr_3 at 25°C; (*b*) Cr_1 at 135°C; (*c*) Cub at 144°C; (*d*) Cub→SmC transition at 161°C; (*e*) SmC at 165 °C; (*f*) isotropic liquid at 166°C.

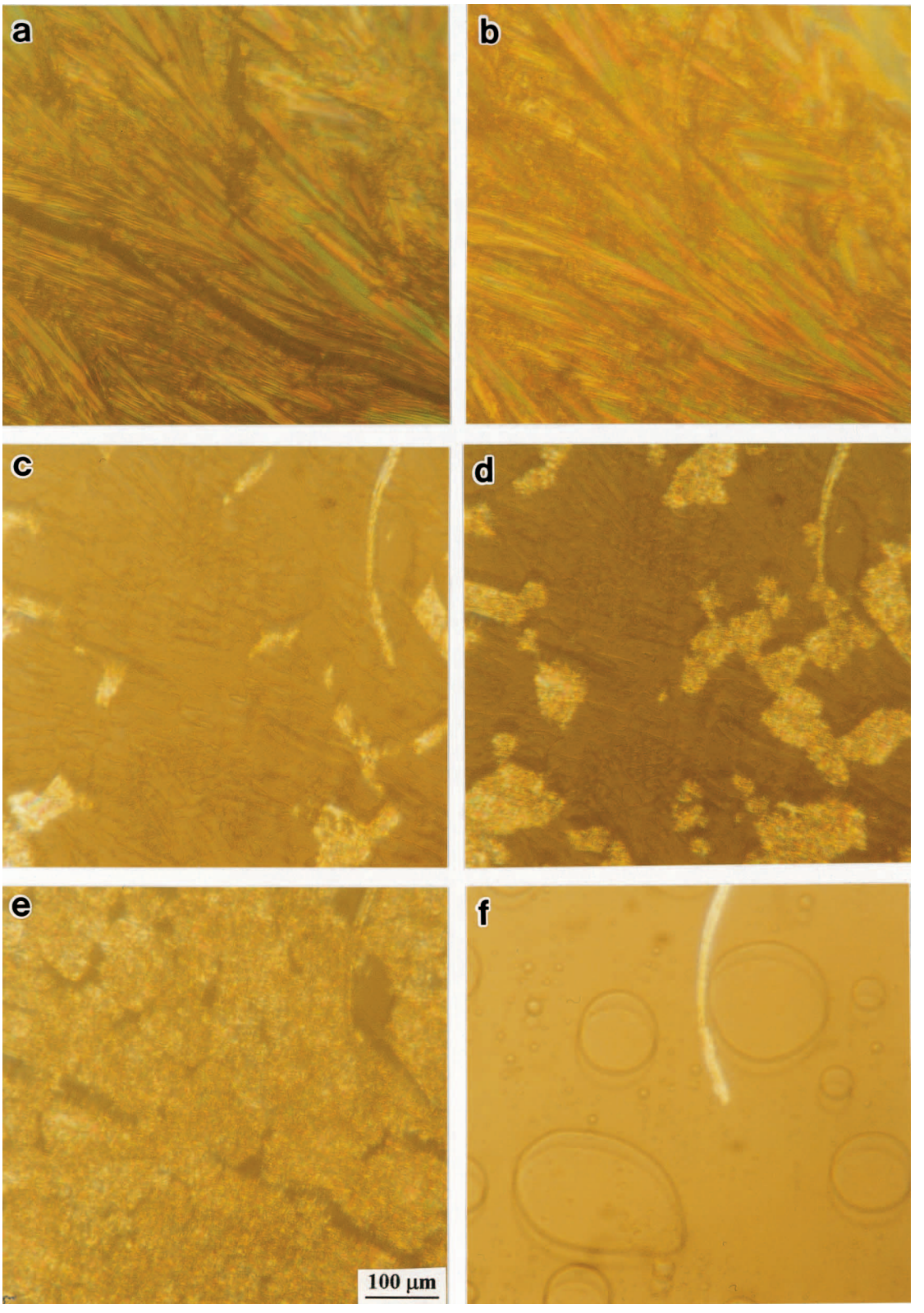

Figure 3. POM micrographs of BABH(10) on heating at 5 MPa: (*a*) Cr_3 at 22°C; (*b*) Cr_1 at 138°C; (*c*,*d*) co-existing sea-island texture of the Cub and SmC phases at 145 and 150°C; (*e*) SmC at 156°C; (*f*) isotropic liquid at 166°C.

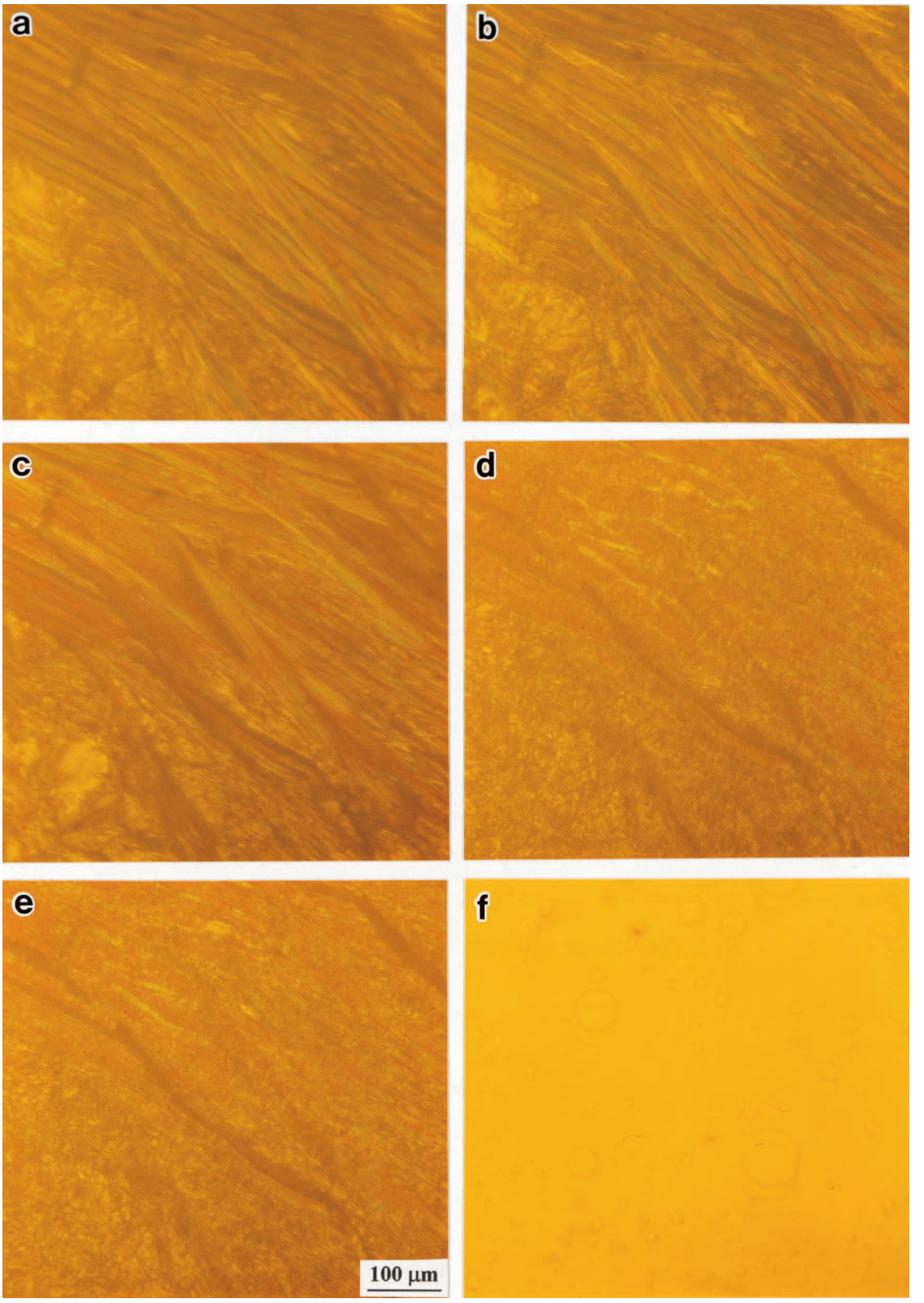

Figure 4. POM micrographs of BABH(10) on heating at 10 MPa: (*a*) Cr_3 at 25°C; (*b*) Cr_2 at 115°C; (*c*) Cr_1 at 138°C; (*d*,*e*) SmC at 145 and 160°C; (*f*) isotropic liquid at 170°C.

changes in texture of BABH(10) at 5 MPa exhibit the same transition sequence of Cr–Cub–SmC–I as observed at atmospheric pressure. The appearance of the coexisting sea-island texture soon after the Cr_1–Cub transition, however, indicates the shifting to lower temperatures of the Cub–SmC transition on applying pressure.

Figure 4 shows the textures of BABH(10) on heating at 10 MPa. Crystalline textures are observed at temperatures up to 138°C (*a–c*). The crystalline texture changes to the wholly sand-like texture of the SmC phase as observed at 145 and 160°C (*d* and *e*). The wholly sand-like texture of the SmC phase remains until isotropization occurs at 167°C (*f*). The dark brown field of view of the cubic phase does not appear between the crystalline phase and isotropic liquid at 10 MPa. On the basis of this series of *in situ* morphological observations at various pressures, the dependence of the transition temperature vs. pressure for BABH(10) is shown in figure 5. The Cr–Cub (or SmC) and SmC–I transition lines are linear in the pressure range observed, while the Cub–SmC transition is observed only in a narrow pressure range between atmospheric and about 4 MPa. The part of this line, shown as dotted, indicates the ambiguous region for the Cub–SmC transition identified by the appearance of the co-existing sea-island texture just after the crystal melting. The transition curves in figure 5 are expressed approximately as linear lines:

Transition	$0 < P < 15$ MPa
$Cr_1 \rightarrow$Cub	$T/°C = 140.3 + 0.330_7$ (P/MPa)
Cub→SmC	$T/°C = 157.4 - 1.334_5$ (P/MPa)
SmC→I	$T/°C = 159.5 + 0.446_9$ (P/MPa).

As is seen also for in BABH(8) [12], the Cub→SmC transition line shows a negative slope in the T vs. P phase diagram of BABH(10). Since the $Cr_1 \rightarrow$Cub and Cub→SmC transition lines have opposite slopes (dT/dP) to each other, the temperature range for the cubic phase decreases with increasing pressure, and the cubic phase disappears at pressures above about 10 MPa. The triple point for the Cr_1, Cub and SmC phases is estimated approximately as 10–11 MPa, 143–144°C. This is an important finding because neither the Cub–SmC transition nor the triple point could be determined by DTA measurements under pressure (see §3.3).

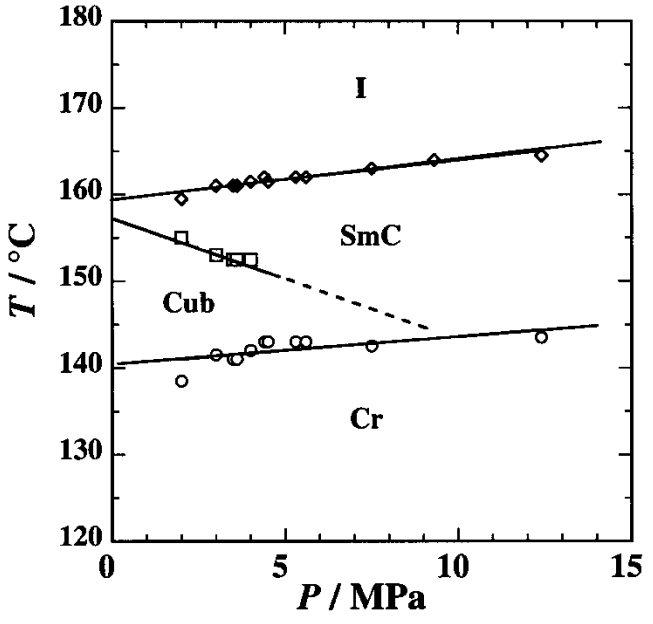

Figure 5. *T–P* phase diagram of BABH(10) constructed in the heating mode using polarizing optical microscopy. The Cub–SmC transition line was clearly determined by POM, while the transition could not be detected by DTA measurements.

Figure 6 shows the X-ray diffraction patterns of the Cub and SmC phases at 140 and 150°C under atmospheric pressure, and the SmC phase at 160°C and 25 MPa. The spot-like pattern (*a*) of the Cub phase at 140°C and atmospheric pressure is similar to that of the Cub phase of BABH(8) reported previously [12]. The observed spots are distributed on the two circles with different radii ($2\theta = 2.98°$, $d = 2.96$ nm; and $2\theta = 3.40°$ $d = 2.59$ nm), which are assigned to the {2 1 1} and {2 2 0} reflections from the various domains of the cubic phase. Separate small angle X-ray studies [15] confirmed the space group *Ia3d* of the cubic phase. Since the X-ray pattern of the SmC phase at 150°C and atmospheric pressure, figure 6 (*b*), shows a Debye–Sherrer ring, this indicates the completely random orientation of the lamellar structures. Thus the Cub–SmC transition can be readily identified by recording the X-ray diffraction pattern. Figure 6 (*c*) shows the diffraction pattern of the sample at 160°C and 25 MPa. The pattern shows two strong arcs on the weak Debye–Sherrer ring, suggesting the occurrence, to some extent of molecular orientation caused by applying pressure. A strong arc is observed at $2\theta \cong 3.00°$ ($d = 2.94$ nm), which is the {0 0 1} reflection of the SmC phase. No spot-like X-ray pattern was recorded in the X-ray measurements of BABH(10) on heating at 25 MPa.

3.3. *Thermal behaviour under pressure*

A high pressure DTA investigation was carried out to explore the effect of pressure on the thermal stability of the cubic and SmC phases. Figure 7 shows the DTA heating curves of BABH(10) at various pressures. The heating curve at 20 MPa shows a sharp peak, a double peak, and a small peak on increasing temperature. Since the *in situ* POM observation detected no

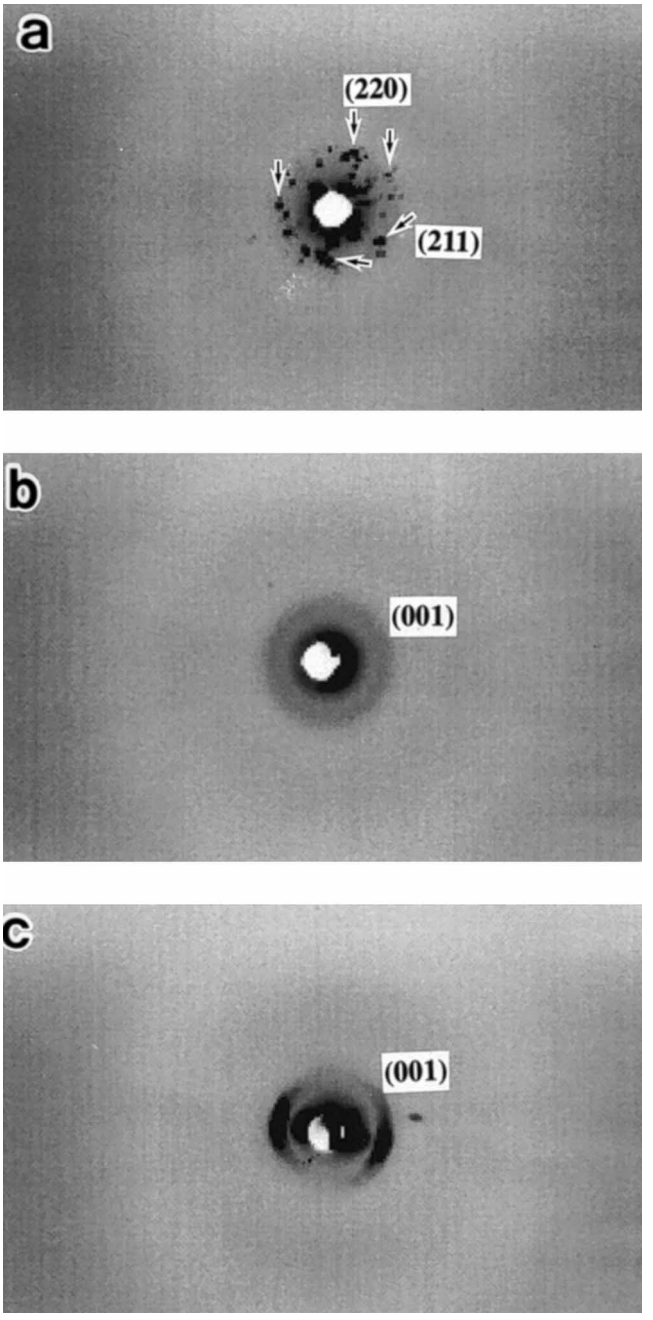

Figure 6. X-ray diffraction patterns of (*a*) the cubic phase at 140°C, atmospheric pressure; (*b*) the SmC phase at 150°C, atmospheric pressure; (*c*) the SmC phase at 160°C, 25 MPa.

Cub–SmC transition under pressures above about 10 MPa, as described, these peaks are the $Cr_3 \rightarrow Cr_2$ transition, the two successive $Cr_2 \rightarrow Cr_1$ and $Cr_1 \rightarrow SmC$ transitions, and the $SmC \rightarrow I$ transition, respectively. The double peak associated with the Cr_2–Cr_1 and Cr_1–SmC transitions merges into an apparently single peak at higher pressures, and at the same time the peak becomes smaller. The quantitative analysis involving

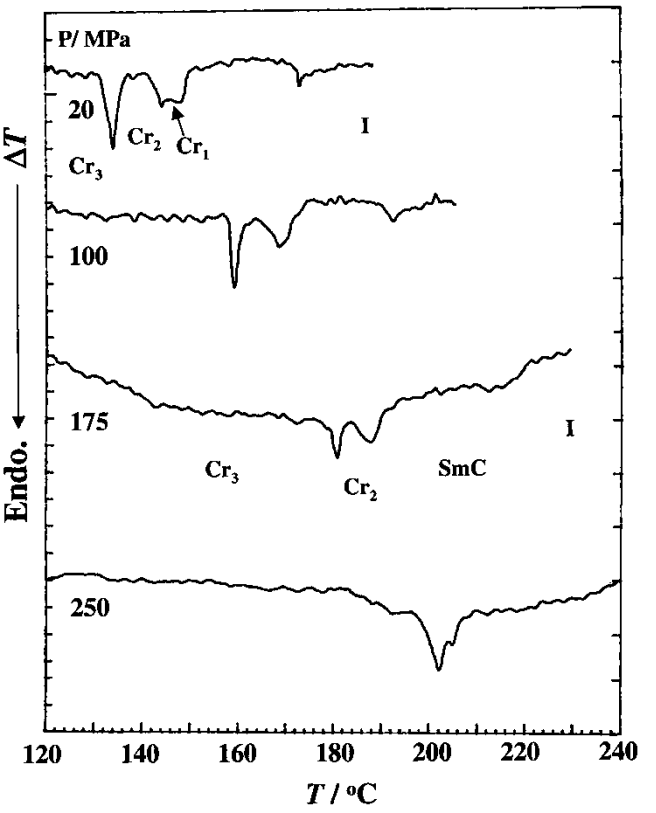

Figure 7. DTA heating curves of BABH(10) at various pressures. Heating rate: 5°C min^{-1}.

the transition enthalpies was not performed as part of this study because the S/N ratio of the DTA curves was poor. The peak temperatures of all the transitions are plotted as a function of pressure in figure 8. The transition curves can be expressed approximately as either first- or second-order polynomials in terms of pressure as:

Transition	(T/°C: peak temperature)
$Cr_3 \rightarrow Cr_2$	$T/°C = 125.1 + 0.371_9 (P/\text{MPa}) - 2.658_8 \times 10^{-4} (P/\text{MPa})^2$
$Cr_2 \rightarrow Cr_1$	$T/°C = 135.8 + 0.357_4 (P/\text{MPa}) - 3.147_6 \times 10^{-4} (P/\text{MPa})^2$
$Cr_1 \rightarrow SmC(Cub)$	$T/°C = 141.7 + 0.285_5 (P/\text{MPa}) - 4.607_2 \times 10^{-5} (P/\text{MPa})^2$
$Cub \rightarrow SmC$	—
$SmC \rightarrow I$	$T/°C = 162.2 + 0.305_0 (P/\text{MPa})$.

In figure 8, the Cub–SmC transition line determined by POM observations is also shown. This line has a large negative slope of $dT/dP = -1.334$ (°C/MPa) in the T vs. P phase diagram and the cubic phase is located in a small triangular region between atmospheric pressure and about 10 MPa. The triple point for the Cr_1, Cub, and SmC phases is estimated approximately as 10–11 MPa and 143–145°C. Since the cubic phase disappears at about 10 MPa, only the SmC phase exists as a mesophase in the high pressure region. Another intersection is predicted from this figure between the Cr_2–Cr_1 and Cr_1–Cub transition lines at

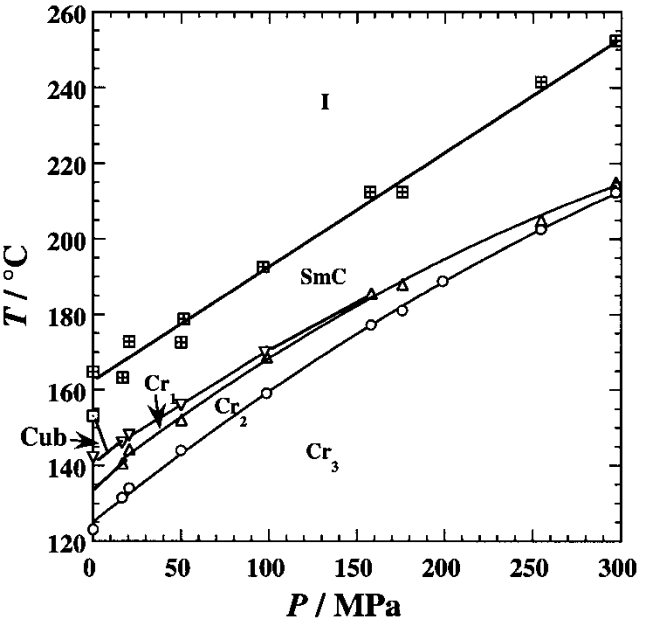

Figure 8. Temperature vs. pressure phase diagram of BABH(10) constructed in the heating mode. The Cub–SmC transition line was determined using polarizing optical microscopy.

about 150–200 MPa, indicating the upper limit of pressure for the Cr_1 phase formation.

The phase diagram constructed in the heating mode exhibits thermodynamically stable phases. On the basis of the thermodynamic data in the table and the (dT/dP) data obtained by high pressure DTA and POM techniques, volume change at the phase transitions can be estimated using the Clausius–Clapeyron equation $dT/dP = \Delta V/\Delta S = T\Delta V/\Delta H$. Since the Cub–SmC transition has a negative slope (dT/dP) and a small, but positive enthalpy of transition ΔH, the volume change is assigned to be negative, i.e. $\Delta V\ (\equiv V_{SmC} - V_{Cub}) < 0$. This means that the molar volume of the SmC phase at high temperatures is smaller than that of the Cub phase at low temperatures, although the ΔV value at the Cub–SmC transition is very small, one decade smaller than that of the Cr_1–Cub transition. It seems reasonable to consider that this relationship holds for the Cub–SmC transition under pressures up to 10–11 MPa. On the other hand, as is shown in figure 8, the temperature interval between the melting and isotropization points is held constant at about 23°C, independent of the disappearance of the Cub phase at high pressures. Thus the thermodynamic relationship between the crystal, SmC phase and isotropic liquid of BABH(10) is essentially stable, irrespective of pressure. This suggests that the Cub phase, located at very low pressures including atmospheric pressure, exists as an unusual one inside the category of lamellar structures (SmC phase in this case), from the point of view of the phase stability.

The prevalence of the SmC phase in place of the cubic phase under pressure is the same trend as seen in BABH(8), indicating the destabilization of the cubic phase under pressure. This behaviour of the Cub and SmC phases in BABH(8) and BABH(10) is illustrated schematically in figure 9 using the criteria of Gibbs energy–T relationship. The Gibbs energy of the Cub phase shifts to higher levels with increasing pressure, while those for the crystal, SmC phase and isotropic liquid slightly change. As a result, the SmC phase is stable between the crystal and the isotropic liquid under higher pressures.

Returning to the relation $\Delta V < 0$, it is quite natural that the Cub→SmC transition occurs when the pressure is increased. Considering the effect of temperature, however, the question arises as to why the molar volume of the SmC phase at the high temperature side is smaller than that of the Cub phase at the low temperature side. On the basis of the thermodynamic analysis of transition entropy for the ANBC

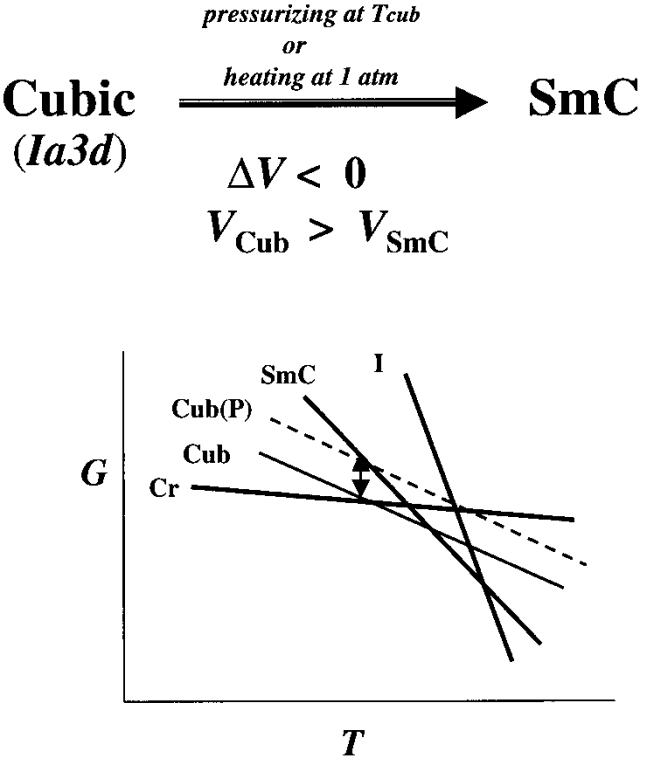

Figure 9. Illustration of the Cub–SmC transition and a schematic diagram of the Gibbs energy–T curve. The effects of pressure on the Cr, SmC, and I phases are neglected for simplicity; they are smaller than that on the Cub phase. The transition line for the Cub phase shifts to higher levels with increasing pressure, indicating the destabilization of the Cub phase on applying pressure.

(4′-*n*-alkoxy-3′-nitrobiphenyl-4-carboxylic acid) and BABH homologues and the quasi-binary picture, Saito and co-workers suggested that the terminal alkoxy chains of these molecules are more disordered in the cubic phase than in the SmC phase, whereas the spatial arrangement of the molecular core is more ordered in the Cub phase than in the SmC phase [16–20]. This suggestion seems to emphasize the existence of highly disordered alkyl chains in the Cub phase, but we feel rather that the molar volume of the cubic phase is primarily governed not by the highly disordered alkyl chains but by the three-dimensionally connected structure itself; the difference between the Cub and lamellar structures is essential for $\Delta V < 0$ [12]. Furthermore, hydrogen bonding between neighbouring BABH molecules should be taken into consideration. For BABH(8) the existence of hydrogen bonding between the core parts of neighbouring molecules is clear in the crystalline phase [4]. Such an interaction, acting perpendicular to the molecular axis direction, is considered to function also as the aggregation force in the formation of the optically isotropic cubic structure. The experimental results reported here suggest that applying pressure to the Cub phase may induce a large strain in the Cub structure formed by the hydrogen bond interaction between the BABH molecules, and as a result of the structure changes into the lamellar structure with an advantageous smaller molar volume (i.e. compact structure) under higher pressure. To support these speculations, we should accumulate more experimental and theoretical knowledge on the Cub phase and its phase behaviour at the molecular level.

4. Conclusion

The phase transition behaviour of BABH(10) was investigated under hydrostatic pressures up to 300 MPa using a high pressure DTA, a polarizing optical microscope equipped with a high pressure optical cell, and a WAXD apparatus equipped with a high pressure vessel. The temperature versus pressure phase diagram was constructed. The phase sequence for BABH(10) can be summarized thus: in the low pressure region below 10 MPa, the transition sequence Cr_3–Cr_2–Cr_1–Cub–SmC–I is seen, and increasing the pressure produces the sequence Cr_3–Cr_2–Cr_1–SmC–I between 10 and 150–200 MPa, and finally the sequence Cr_3–Cr_2–SmC–I is obtained in the high pressure region. The Cub–SmC transition was clearly observed using the high pressure POM and WAXD apparatus. The dark field of view for the optically isotropic Cub phase changes reversibly to and from the sand-like texture of the SmC phase both under isobaric and isothermal conditions. The spot-like X-ray pattern of the Cub phase at atmospheric pressure changes reversibly to and from the Debye–Sherrer ring pattern of the SmC phase at high pressures above 10–20 MPa. In the phase diagram constructed from POM, the Cub–SmC transition line has a large negative slope. The triple point for the Cr_1, Cub and SmC phases is estimated to be at 10–11 MPa and 143–145°C, indicating the upper limit of pressure for cubic phase formation.

S.K. is grateful for financial support from the Ministry of Education, Culture, Sports, Science, and Technology, Japan [Grant-in-Aid for Scientific Research on Priority Areas (A), No. 413/13031037 and 14045232, and Scientific Research (C) 14550846].

References

[1] Gray, G. W., Jones, B., and Marson, F., 1957, *J. chem. Soc.*, 393.
[2] Schubert, H., Hauschild, J., Demus, D., and Hoffmann, S., 1978, *Z. Chem.*, **18,** 256.
[3] Demus, D., Gloza, A., Hartung, H., Hauser, A., Rapthel, I., and Wiegeleben, A., 1981, *Cryst. Res. Technol.*, **16,** 1445.
[4] Göring, P., Diele, S., Fischer, S., Wiegeleben, A., Pelzl, G., Stegemeyer, H., and Thyen, W., 1998, *Liq. Cryst.*, **25,** 467.
[5] Luzzati, V., and Spegt, A., 1967, *Nature*, **215,** 701.
[6] Tardieu, A., and Billard, J., 1976, *J. Phys. (Paris) Coll.*, **37,** C3–79.
[7] Levelut, A.-M., and Fang, Y., 1991, *Colloq. Phys.*, **23,** C7–229.
[8] Levelut, A.-M., and Clerc, M., 1998, *Liq. Cryst.*, **24,** 105.
[9] Morimoto, N., Saito, K., Morita, Y., Nakasuji, K., and Sorai, M., 1999, *Liq. Cryst.*, **26,** 219.
[10] Saito, K., Sato, A., Morimoto, N., Yamamura, Y., and Sorai, M., 2000, *Mol. Cryst. liq. Cryst.*, **347,** 249.
[11] Saito, K., Shinhara, T., and Sorai, M., 2000, *Liq. Cryst.*, **27,** 1555.
[12] Maeda, Y., Saito, K., and Sorai, M., 2003, *Liq. Cryst.*, **30,** 1139.
[13] Maeda, Y., and Kanetsuna, H., 1985, *Bull. Res. Inst. Polym. Tex.*, **149,** 119; Maeda, Y., 1990, *Thermochim. Acta.*, **163,** 211.
[14] Maeda, Y., and Koizumi, M., 1996, *Rev. sci. Instrum.*, **67,** 2030; Maeda, Y., and Koizumi, M., 1998, *Rev. high pressure Sci. Technol.*, **7,** 1532.
[15] Kutsumizu, S., Saito, K., and Ito, T. to be published.
[16] Saito, K., Sato, A., and Sorai, M., 1998, *Liq. Cryst.*, **25,** 525.
[17] Sato, A., Yamamura, Y., Saito, K., and Sorai, M., 1999, *Liq. Cryst.*, **26,** 1185.
[18] Saito, K., and Sorai, M., 2002, *Chem. phys. Lett.*, **366,** 56.
[19] Saito, K., Shinhara, T., Nakamoto, T., Kutsumizu, S., Yano, S., and Sorai, M., 2002, *Phys. Rev. E*, **65,** 031719.
[20] Sorai, M., and Saito, K., 2003, *Chem. Rec.*, **3,** 29.